J. Fluid Mech. (2008), *vol.* 617, *pp.* 231–253.
doi:10.1017/S0022112008004096 Printed in the United Kingdom

Low-frequency sound sources in high-speed turbulent jets

DANIEL J. BODONY[1,†] AND SANJIVA K. LELE[1,2]

[1]Center for Turbulence Research, Stanford, CA, USA

[2]Department of Mechanical Engineering and Department of Aeronautics and Astronautics, Stanford University, Stanford, CA, USA

(Received 13 March 2007 and in revised form 25 August 2008)

An analysis of the sound radiated by three turbulent, high-speed jets is conducted using Lighthill's acoustic analogy (*Proc. R. Soc. Lond.* A, vol. 211, 1952, p. 564). Computed by large eddy simulation the three jets operate at different conditions: a Mach 0.9 cold jet, a Mach 2.0 cold jet and a Mach 1.0 heated jet. The last two jets have the same jet velocity and differ only by temperature. None of the jets exhibit Mach wave characteristics. For these jets the comparison between the Lighthill-predicted sound and the directly computed sound is favourable for all jets and for the two angles (30° and 90°, measured from the downstream jet axis) considered. The momentum ($\rho u_i u_j$) and the so-called entropy [$p - p_\infty - a_\infty^2(\rho - \rho_\infty)$] contributions are examined in the acoustic far field. It is found that significant phase cancellation exists between the momentum and entropy components. It is observed that for high-speed jets one cannot consider $\rho u_i u_j$ and $(p' - a_\infty^2 \rho')\delta_{ij}$ as independent sources. In particular the $\rho' \overline{u}_x \overline{u}_x$ component of $\rho u_i u_j$ is strongly coupled with the entropy term as a consequence of compressibility and the high jet velocity and not because of a linear sound-generation mechanism. Further, in more usefully decoupling the momentum and entropic contributions, the decomposition of T_{ij} due to Lilley (*Tech. Rep.* AGARD CP-131 1974) is preferred. Connections are made between the present results and the quieting of high-speed jets with heating.

1. Introduction

There continues to be a gap in the understanding of the sources of jet noise and of their dependence on external conditions, such as those determined by the nozzle and the environment farther upstream. The influence of nozzle chevrons on the radiated sound is, for example, still parametrically characterized based on a series of experimental studies (Saiyed, Mikkelsen & Bridges 2003, for example). Further development of an understanding of the 'sound sources' in a high Reynolds number jet, however, is slowed for two primary reasons: (i) the lack of a universally agreed upon acoustic theory and (ii) the difficulty in making experimental measurements suggested by the acoustic theories. The current theories, most notably those of Lighthill (1952), Lilley (1974) and Goldstein (2003), are similar in their arbitrary, but exact, rearrangement of the Navier–Stokes equations (with new variables in the case of Goldstein) and in the functional form of the corresponding source term.

† Present address and address for correspondence: Department of Aerospace Engineering, University of Illinois at Urbana-Champaign, IL, USA; bodony@illinois.edu.

The semi-empirical theory of Tam & Auriault (1999) defines its own source term. In general, each analogy defines its *own* acoustic source to be of the form

$$\{\text{linear combination of } \partial_t \text{ and } \partial_{x_i}\}\, S_j(\boldsymbol{x}, t),$$

where S_j may involve additional differentiation. There are two points regarding S_j. First, its physical meaning must be investigated and connected to the underlying fluid motion through careful study of model problems. Second, measurements of S_j are quite difficult, and currently, only point measurements of related quantities have been obtained (Panda & Seasholtz 2002; Panda *et al.* 2004, for example). At present it appears that the major practical difference between the dominant theories (when used with a high-fidelity simulation for prediction) is in their sensitivity to numerical errors (Samanta *et al.* 2006).

Large eddy and direct numerical computational studies of jet noise offer an alternative to experimental measurements for examining the sources of noise in turbulent flows. The direct numerical simulation (DNS) of Freund (2001) continues to be the only calculation of its type; post-processing of the DNS data has been useful in evaluating key assumptions (e.g. Khavaran, Bridges & Freund 2002). However the high cost, low Reynolds number and single jet operating point of the DNS calculation are limiting.

The large eddy simulation (LES) technique has been used for predicting the noise from high Reynolds number turbulent jets. One of the earliest uses of LES for jet noise prediction was by Gamet & Estivalezes (1998) for a high-speed, high-temperature jet. Later investigators (Boersma & Lele 1999; Bogey, Bailly & Juvé 2000; Constantinescu & Lele 2001) focused on the low Reynolds number, Mach 0.9, unheated jet, using the the experimental data of Stromberg, McLaughlin & Troutt (1980). The importance of boundary conditions, specifically the inflow condition, has recently been discussed (Bogey & Bailly 2005) as have the use of implicit subgrid scale models in lieu of a more traditional modelling approach (Bogey & Bailly 2003; Andersson, Eriksson & Davidson 2005*a*; Shur, Spalart & Strelets 2005*a*), although the influence of the latter on the far field sound remains an open question (Bodony & Lele 2008).

The method has also been applied to increasingly complex geometries (see e.g. Andersson, Eriksson & Davidson 2005*b*; Shur *et al.* 2005*a*, *b*, 2006; Uzun & Hussaini 2007; Viswanathan *et al.* 2008), in examining the effect of laminar vs turbulent boundary exiting the nozzle (Barré, Bogey & Bailly 2006) and in investigating the flow in the vicinity of the nozzle lip (Uzun & Hussaini 2007). A more detailed review of the use of LES in the prediction of jet noise may by found in Bodony & Lele (2008).

There have been limited studies utilizing the databases of high-fidelity LES of turbulent jets to examine the noise sources. Rembold & Kleiser (2004), for example, examined Lighthill's stress tensor T_{ij} for a rectangular jet. Bogey & Bailly (2007) used causality methods to cross-correlate the far field pressure with near field events in a manner similar to the work of Panda and colleagues (Panda & Seasholtz 2002; Panda *et al.* 2004). In particular they explored the dependence of the correlations on the jet Mach and Reynolds numbers. Brusniak, Shur & Spalart (2006) used phased array techniques to map out the array-predicted noise source region, while Viswanathan *et al.* (2007) used an elliptical mirror. Lew, Blaisdell & Lyrintzis (2007) used their LES databases of low-speed heated and unheated jets to examine the Lighthill noise sources in a manner similar to Freund (2003) while focusing on the entropy term contribution to the noise of low-speed hot jets. Lew *et al.* (2007) found that the entropy noise contribution dominates the noise spectra at all angles for their lowest

speed jet. In addition the entropy and linear 'shear noise' terms are strongly anti-correlated for an observer at 30° but show little correlation for an observer at 90°. They also observed that heating a constant-velocity jet changes the nature of the momentum–entropy correlation by an amount dependent on U_j. Finally they note that the spectral shapes of the individual components of T_{ij} can differ markedly from the overall spectrum.

1.1. *Objectives*

The objectives of this work are to conduct a detailed analysis of Lighthill's acoustic analogy to high-speed turbulent jets. We critically examine the consequences of the Lighthill stress tensor and seek to provide some insight into the use of T_{ij} in noise-modelling efforts. It will be shown that the momentum $\rho u_i u_j$ and so-called entropy term $[p - p_\infty - a_\infty^2(\rho - \rho_\infty)]\delta_{ij}$ become nearly perfectly anti-correlated for the Mach numbers we consider. We then explain this result for jets that do not exhibit Mach wave radiation. A comment on the effects of heating closes the discussion. This work extends a previous study by the authors (Bodony & Lele 2005).

To accomplish our objectives we first summarize in the Appendix the validation of the LES results against experimental data for the near and far fields, including a comparison of the Lighthill-predicted sound spectra to the directly computed sound spectra from the compressible LES calculations to establish their validity. We then examine in more detail the spectra associated with the components of the Lighthill source term.

2. Sound predictions using Lighthill's theory

2.1. *Previous work*

Lighthill's theory in numerical jet noise prediction has been used previously. For a plane (two-dimensional) jet Bastin, Lafon & Candel (1997) found that the source $S = \partial_{x_i}\partial_{x_j}T_{ij}$, where

$$T_{ij} = \rho u_i u_j + \left[(p - p_\infty) - a_\infty^2(\rho - \rho_\infty)\right]\delta_{ij} - \tau_{ij} \tag{2.1}$$

is the Lighthill quadrupole amplitude, yielded inferior sound predictions relative to the alternative far field expression involving $\ddot{T}_{ij}$ or the associated twice-integrated by parts form. In his round jet Freund (2001) found, using the identity

$$S = \frac{\partial^2}{\partial t^2}(\rho - \rho_\infty) - a_\infty^2 \frac{\partial^2}{\partial x_j \partial x_j}(\rho - \rho_\infty), \tag{2.2}$$

that noise predictions using Lighthill's theory compared well with the instantaneous pressure time history. Later Freund (2002) showed that the Lighthill-predicted noise spectrum at $\Theta = 30°$ compared well with the DNS data and with the data of Stromberg *et al.* (1980). (See figure 1 for the definition of the polar angle Θ.) Freund also discussed the relative roles of the 'shear noise', 'self noise' and 'entropy' terms embedded in T_{ij} and noted their statistical dependence at observer angles close to the downstream jet axis. The work of Lew *et al.* (2007) revisited the analysis of Freund (2003) for lower speed heated and unheated turbulent jets; in particular they examined the role of the entropy term in hot, low-speed jets.

2.2. *Frequency domain considerations*

In this section we document how the space–time databases generated from the LESs presented in the Appendix are used to examine Lighthill's theory for high-speed jets in the frequency domain.

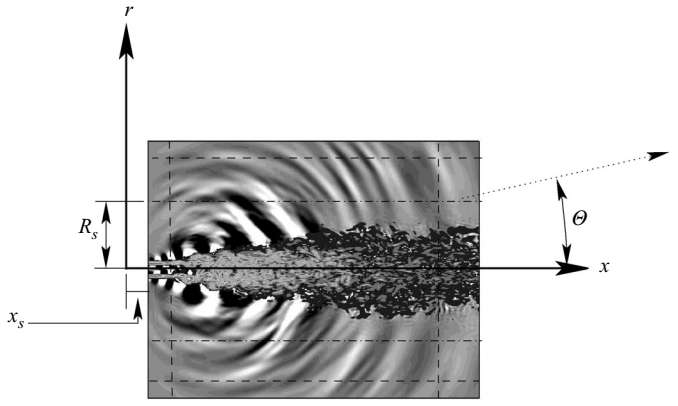

FIGURE 1. Schematic of calculation domain showing major features. The central region contains the LES domain and the sponge (— — —) and Kirchhoff surface surfaces (— · — · —).

The calculation of the far field sound using Lighthill's theory begins by considering the integral form of the time Fourier transformed version of (2.2),

$$\rho \widehat{-\rho_\infty}(\boldsymbol{x};\omega) := \widehat{\rho'}(\boldsymbol{x};\omega) = \frac{1}{4\pi a_\infty^2} \int_{\mathscr{R}^3} \frac{\mathrm{e}^{\mathrm{i}\omega R/a_\infty}}{R} \hat{S}(\boldsymbol{y};\omega)\,\mathrm{d}\boldsymbol{y}, \tag{2.3}$$

where $R = |\boldsymbol{x} - \boldsymbol{y}|$ and $\hat{S}$ is the transformed source. The advantage of using the frequency domain form of (2.3) and not its time domain analog is in avoiding the interpolation needed for the evaluation of S at the retarded time $t - R/a_\infty$. An alternative form which follows from twice integrating (2.3) by parts (and assuming the boundary terms vanish for a surface taken to infinity) is

$$\widehat{\rho'}(\boldsymbol{x};\omega) = \frac{1}{4\pi a_\infty^2} \int_{\mathscr{R}^3} \frac{\partial^2}{\partial y_i \partial y_j} \left\{ \frac{\mathrm{e}^{\mathrm{i}\omega R/a_\infty}}{R} \right\} \hat{T}_{ij}(\boldsymbol{y};\omega)\,\mathrm{d}\boldsymbol{y}, \tag{2.4}$$

where the quadrupole Fourier amplitude $\hat{T}_{ij}$ now appears explicitly.

In view of (2.1) the resultant density Fourier amplitudes can be considered as the sum of the components

$$\widehat{\rho'}_{tot} = \widehat{\rho'}_{mom} + \widehat{\rho'}_{ent} + \widehat{\rho'}_{vis},$$

where

$$\widehat{\rho'}_{mom}(\boldsymbol{x};\omega) = \frac{1}{4\pi a_\infty^2} \int_{\mathscr{R}^3} \frac{\partial^2}{\partial y_i \partial y_j} \left\{ \frac{\mathrm{e}^{\mathrm{i}\omega R/a_\infty}}{R} \right\} \widehat{\rho u_i u_j}(\boldsymbol{y};\omega)\,\mathrm{d}\boldsymbol{y}, \tag{2.5}$$

$$\widehat{\rho'}_{ent}(\boldsymbol{x};\omega) = \frac{1}{4\pi a_\infty^2} \int_{\mathscr{R}^3} \frac{\partial^2}{\partial y_j \partial y_j} \left\{ \frac{\mathrm{e}^{\mathrm{i}\omega R/a_\infty}}{R} \right\} \left(\widehat{p'} - a_\infty^2 \widehat{\rho'}\right)(\boldsymbol{y};\omega)\,\mathrm{d}\boldsymbol{y} \tag{2.6}$$

and

$$\widehat{\rho'}_{vis}(\boldsymbol{x};\omega) = \frac{-1}{4\pi a_\infty^2} \int_{\mathscr{R}^3} \frac{\partial^2}{\partial y_i \partial y_j} \left\{ \frac{\mathrm{e}^{\mathrm{i}\omega R/a_\infty}}{R} \right\} \widehat{\tau}_{ij}(\boldsymbol{y};\omega)\,\mathrm{d}\boldsymbol{y}. \tag{2.7}$$

The viscous term is expected to be at least a factor of the Reynolds number smaller than the momentum term (Crighton 1975) and is thus negligible for our simulations which are devoid of solid boundaries, as confirmed by Freund (2003) in

ID	Δt	Samples, N	ΔSt	St_{max}
M09TR086	$0.10r_0/a_\infty$	8 192	0.0030	11.98
M15TR056	$0.10r_0/a_\infty$	8 192	0.0016	6.67
M15TR230	$0.05r_0/a_\infty$	12 000	0.0022	13.33

TABLE 1. Details of the time series resolution of the jet LES databases.

his low Reynolds number jet; hence, we take $\widehat{\rho'}_{vis} \equiv 0$. We also do not consider the contribution of the subgrid scale stresses to the Lighthill-determined acoustic spectra and focus solely on the sound due to the resolved field.

From the definitions of $\widehat{\rho'}_{tot}$, $\widehat{\rho'}_{mom}$ and $\widehat{\rho'}_{ent}$ given above we form the appropriate spectra $S_{\rho\rho,tot}(\omega)$, $S_{\rho\rho,mom}(\omega)$ and $S_{\rho\rho,ent}(\omega)$, using the properties of the fast Fourier transform and averaging (see § 2.3). From these spectra the corresponding sound pressure levels (SPLs) are computed as

$$\mathrm{SPL} = 10\log_{10}\left(\frac{S_{\rho\rho,tot}}{p_{ref}^2}\right)$$

with similar definitions for the momentum and entropy terms. We take $p_{ref} = 20$ μPa. Note that the cross-correlations between the momentum and entropy contributions are naturally taken into account, since $S_{\rho\rho,tot}(\omega)$ is computed using the full density fluctuation ρ'_{tot}.

2.3. *Numerical aspects*

In practice one must perform certain numerical operations to use (2.4): (i) fast Fourier transform (which requires windowing in time) and (ii) numerical quadrature. For the windowing in time of T_{ij} the weighting presented by Freund (2001) is used. Given the time history of T_{ij}, the windowed version $\tilde{T}_{ij}$ is computed according to $\tilde{T}_{ij}(\boldsymbol{x}, t) = w_t(t)T_{ij}(\boldsymbol{x}, t)$, where

$$w_t = \frac{1}{2}\left(\tanh\left[\frac{5(t-t_1)}{t_1-t_0}\right] + \tanh\left[\frac{5(t_2-t)}{t_f-t_2}\right]\right) \tag{2.8}$$

for a time record $t_0 \leqslant t \leqslant t_f$. With t_1 and t_2 given by $t_1 = 0.2(t_f - t_0) + t_0$ and $t_2 = 0.8(t_f - t_0) + t_0$ the frequencies over which the weighting distorts the spectrum of $\tilde{T}_{ij}$, relative to the original data, are confined to $St \leqslant 0.02$; for $St > 0.02$ the spectra are unaffected by w_t. The time histories of the three LES jets were saved in constant time step increments. Table 1 gives the time and frequency discretization of the databases. For each simulation a large number of flow samples were taken, ranging from $N = 8\,192$ to $N = 12\,000$, depending on the case. The sample rate is case dependent but corresponds to a maximum Strouhal number St_{max} of at least 6.67, well beyond the grid-limited value of $St \approx 1.5$. To maintain a reasonable sample size for frequencies below $St = 0.1$ we use the entire sample in one segment in the calculation of the fast Fourier transform. The subsequent periodograms are bin-averaged over a width $\Delta St = 0.015$ and over the homogeneous azimuthal direction to construct the spectra.

The quadrature used simple trapezoidal integration in all directions and was performed in cylindrical coordinates over the domain $(x, r) \in [0, 31]D \times [0, 12.5]D$. The trapezoidal method was found to be superior to the methods (Simpson's rule, for example) which rely on higher order interpolating polynomials and can suffer from the Runge phenomenon associated with highly oscillatory integrands (Isaacson & Keller

1966). The three-dimensional integration was performed as repeated one-dimensional integrations.

3. Observations

Comparisons of the far field predictions of the pressure spectra are presented in the Appendix using the integral form of Lighthill's analogy (2.4) and the previously used Kirchhoff surface predictions.

For each jet the individual contributions to the total spectrum by the momentum term (2.5) and the entropy term (2.6) are presented in detail next. The decomposition due to Lilley (1974), which is the time-integrated form of (24) in his work,

$$p - p_\infty - a_\infty^2(\rho - \rho_\infty) = \underbrace{-\frac{\gamma - 1}{2}\rho u_k u_k}_{\text{term I}} + \underbrace{a_\infty^2 \int \frac{\partial}{\partial x_k}\left[\rho u_k \left(\frac{h_\infty - h_s}{h_\infty}\right)\right] \mathrm{d}t}_{\text{term II}}, \qquad (3.1)$$

with h_∞ and h_s being the free stream and stagnation enthalpies, is used to further examine the spectra. Such a decomposition was also used by Freund (2003) for his Mach 0.9 jet.

Figure 2 shows the decomposition for the unheated Mach 0.9 jet. At 30° the momentum term over-contributes to the overall sound pressure level (OASPL) by roughly 2 dB for frequencies up to $St = 0.3$, as also found by Freund (2003). At higher frequencies, a general trend cannot be stated. Beyond $St = 0.8$ the momentum and entropy terms become of similar magnitude, with the momentum term being of larger amplitude for all available frequencies. Around $St = 0.25$ the term I and term II contributions to the entropy term exchange dominance, with term II being the most significant at higher frequencies. At 90° the momentum clearly dominates the total spectrum, being at least 10 dB above the entropy contribution.

For the cold Mach 2 jet (figure 3) at 30° the Lighthill-predicted spectra are of a different nature than for the Mach 0.9 cold jet; at 90° the high-speed jet spectra are qualitatively the same as for the lower speed jet. Figure 3(*a*) shows that (i) there is much greater $(\rho u_i u_j)$–$(p' - a_\infty^2 \rho')$ cancellation at all frequencies, and (ii) the peak frequencies of the individual spectra near $St = 1$ do not correspond to the peak frequency of the total spectrum's peak of $St = 0.3$. (There does, however, appear to be a weak local maximum near $St = 0.3$ for the individual spectra.) Below $St = 0.4$ the momentum stress term is approximately 3–8 dB greater than the total SPL, indicating cancellation with the entropy term. For frequencies of $St < 0.4$ we observe that term I $\gg$ term II for the entropy contribution; at higher frequencies they are of comparable magnitude. At $St = 0.4$ and above the $\rho u_i u_j$ and $(p' - a_\infty^2 \rho')\delta_{ij}$ contributions become increasingly anti-correlated to yield a total SPL which is much less than the individual SPLs. Conversely, for $St \geqslant 0.4$, the term I and term II portions of $p' - a_\infty^2 \rho'$ show constructive interference. The rather marked difference between the $(\rho u_i u_j)$ and $(p' - a_\infty^2 \rho')$ spectra at 30° was observed by Lew *et al.* (2007) for lower speed jets and will be discussed in detail later.

Turning to the 90° spectrum in Figure 3(*b*) we observe that it is the momentum stress that is the dominant source of the radiated noise for the range of frequencies available. The entropy term contributes very little at all frequencies. The spectral peak occurs near $St = 0.3$ for all individual spectra and for the total spectrum.

When the Mach 1 heated jet, with $T_j/T_\infty = 2.3$, is considered in figure 4 we observe a different picture than for the unheated jet at the same velocity in some important

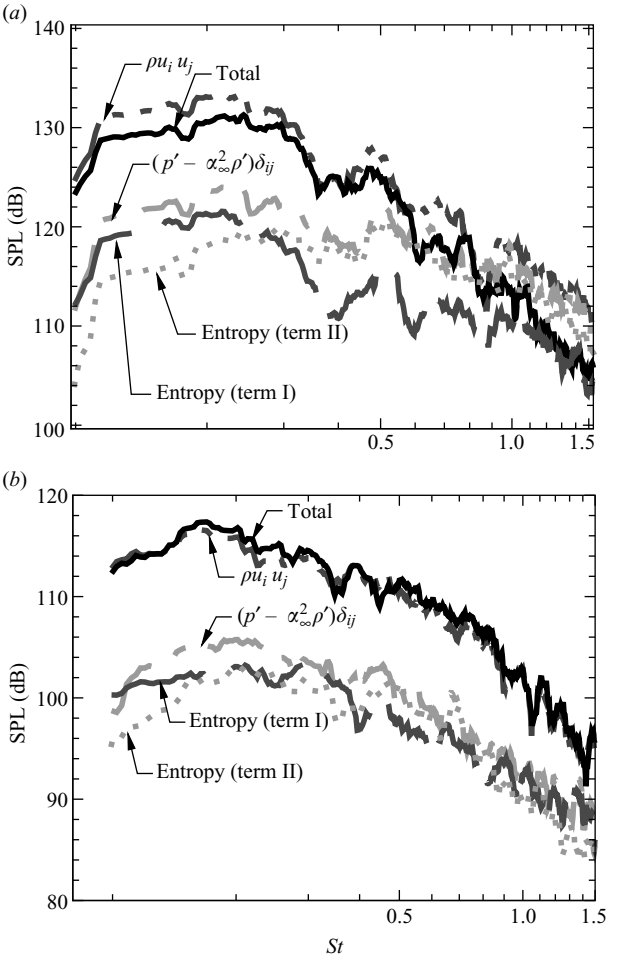

FIGURE 2. Narrowband spectra at $\mathscr{R} = 30D_j$ for the Mach 0.9 unheated jet M09TR086. — total; — · · — $\rho u_i u_j$; — · — $p' - a_\infty^2 \rho'$; — — entropy (term I); · · · entropy (term II). (*a*) $\theta = 30°$, (*b*) $\theta = 90°$.

aspects. At 30° the heated jet's component spectra show a St peak well beyond the peak frequency of the total spectrum, although there is the minor local maximum near $St = 0.2$ in the individual spectra. Over *all* frequencies the $\rho u_i u_j$ and $p' - a_\infty^2 \rho'$ contributions are closely correlated, especially at higher frequencies, and it is now the term II component that is most important. Indeed term I, $-[(\gamma - 1)/2]\rho u_k u_k$, seems to play very little role. At 90° the momentum and term II components combine constructively for the total SPL for $St < 0.4$ but add destructively for higher frequencies. At both angles the decay of the total SPL with increasing St shows a different functional form than do the individual spectra.

4. Discussion

From the aforementioned observations there are additional aspects of the Lighthill-predicted sound spectra that are worth discussing in greater detail. The first is the difference in the 30° individual component spectra and the total spectrum for the

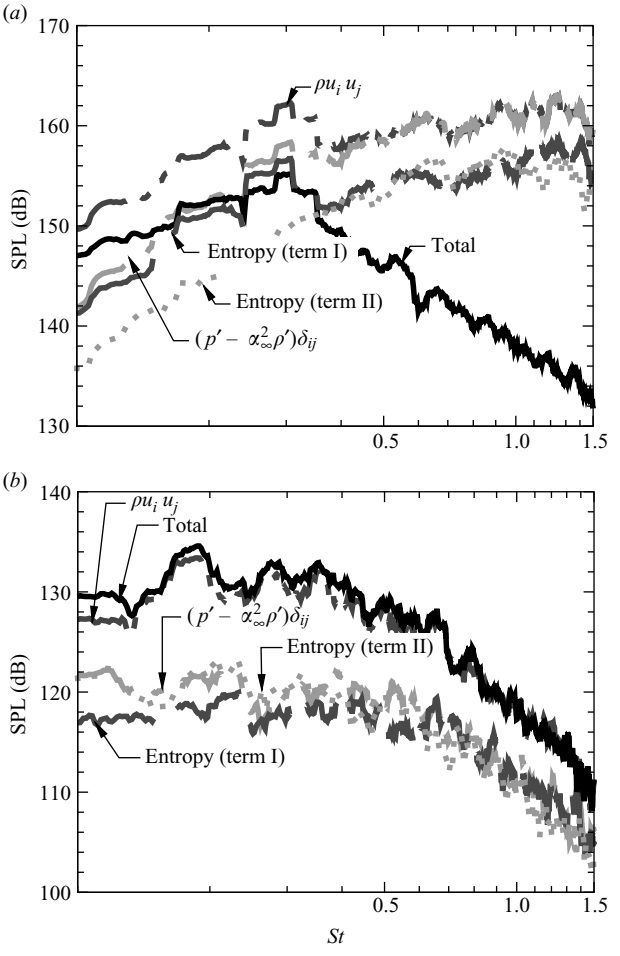

FIGURE 3. Narrowband spectra at $\mathscr{R} = 30D_j$ for the Mach 2.0 unheated jet M15TR056: — total; — · · — $\rho u_i u_j$; — · — $p' - a_\infty^2 \rho'$; — — entropy (term I); · · · entropy (term II). (*a*) $\theta = 30°$, (*b*) $\theta = 90°$.

high-speed jets as shown in figures 3(*a*) and 4(*a*). The second is the amount of cancellation that occurs for the high-speed jets between the momentum and entropic contributions.

4.1. *High-speed jet spectra at* $\Theta = 30°$ *and* $90°$

The Mach 2.0 unheated and Mach 1.0 heated jets exhibit qualitatively different spectra at 30° for the *individual* components of $\hat{T}_{ij}$ compared to their sum, in contrast to the Mach 0.9 cold jet as found here (figure 2) and earlier by Freund (2003). To examine the cause consider the further decomposition of the momentum term $\rho u_i u_j$ into

$$\rho u_i u_j = \overline{\rho}\,\overline{u}_i\overline{u}_j + \underbrace{\overline{\rho}(\overline{u}_i u_j' + u_i'\overline{u}_j)}_{L_1} + \underbrace{\rho'\overline{u}_i\overline{u}_j}_{L_2} + \underbrace{\rho'(\overline{u}_i u_j' + u_i'\overline{u}_j)}_{Q_1} + \underbrace{\overline{\rho}u_i'u_j'}_{Q_2} + \underbrace{\rho'u_i'u_j'}_{C}, \quad (4.1)$$

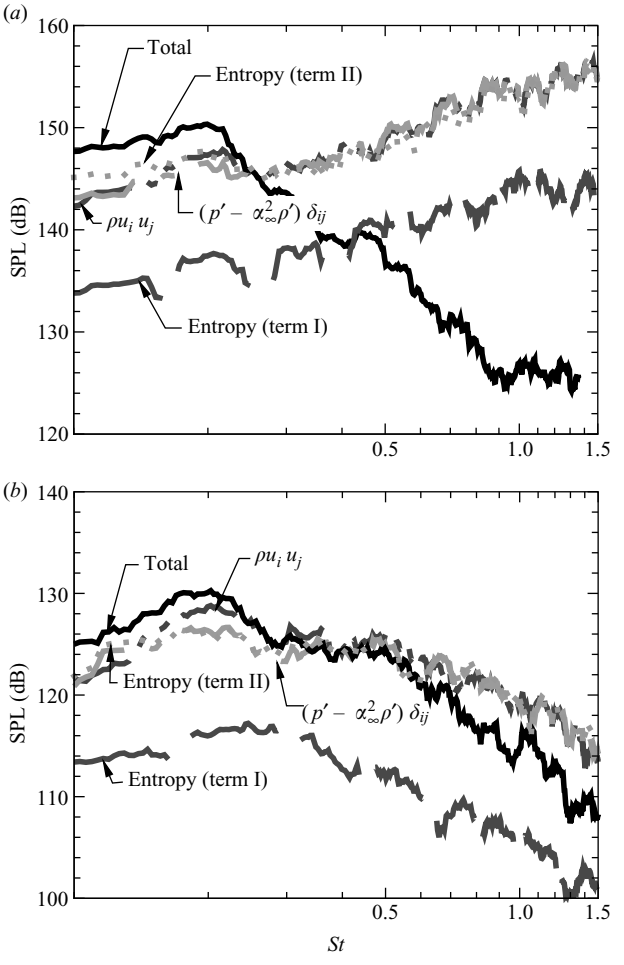

FIGURE 4. Narrowband spectra at $\mathscr{R} = 30D_j$ for the Mach 1.0 heated jet M15TR230: — total; — · · — $\rho u_i u_j$; — · — $p' - a_\infty^2 \rho'$; — — entropy (term I); · · · entropy (term II). (*a*) $\theta = 30°$, (*b*) $\theta = 90°$.

where an overbar denotes a time-averaged quantity with corresponding fluctuation denoted by the prime. The terms L_1† and L_2 are linear in the fluctuations; Q_1 and Q_2 are quadratic in the fluctuations; and C is cubic. The very first term, $\overline{\rho}\,\overline{u}_i\overline{u}_j$, has only a mean component and does not radiate sound; it is not considered further. The far field spectra for the five remaining terms are plotted in figure 5 for the Mach 2 cold jet and in figure 6 for the Mach 1 heated jet. Note that the decomposition of (4.1) is more general than that used by Freund (2003).

† Clearly the individual terms of (4.1) are second-order tensors and formally require two indices. For the purposes of discussion we associate L_1 with the sound generated by the twice-contracted quantity $(\partial^2(\mathrm{e}^{\mathrm{i}\omega R/a_\infty}/R)/\partial y_i \partial y_j)\overline{\rho}(\overline{u}_i u_j' + u_i'\overline{u}_j)$. Thus our statement that $L_1 = \overline{\rho}(\overline{u}_i u_j' + u_i'\overline{u}_j)$ implies contraction over i and j and convolution with the Green's function. The same convention is used for L_2, Q_1, Q_2 and C. In the sense used here, L_1, L_2, etc. denote not the values of the 'source terms' but rather their contribution to far field sound at selected observer locations.

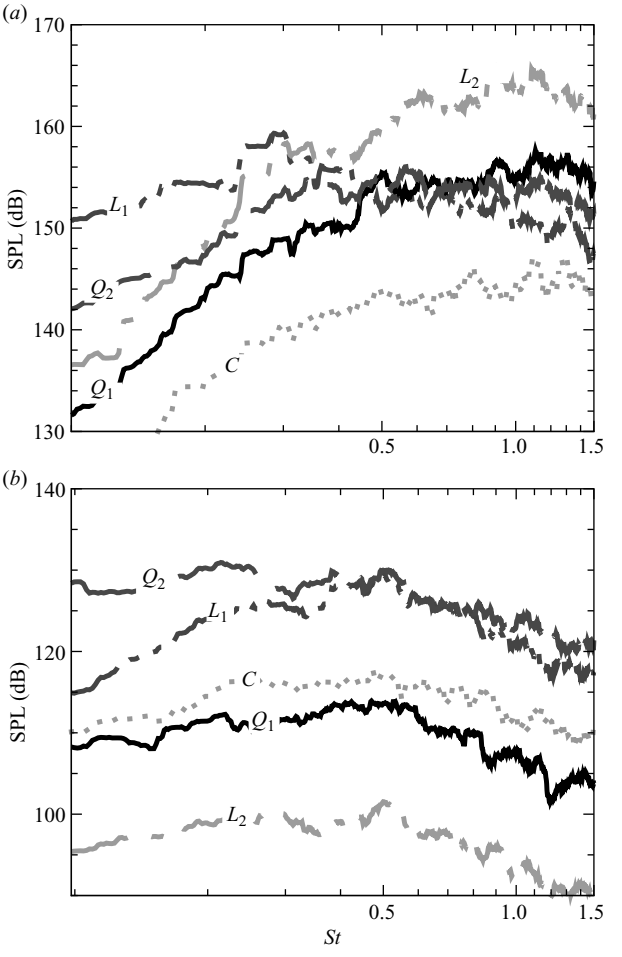

FIGURE 5. Component spectra contributing to the spectrum of $\rho u_i u_j$ for the jet M15TR056: $-\cdot\cdot-L_1$; $-\cdot-L_2$; — Q_1; $-\,-\,Q_2$; $\cdots C$; $-\blacktriangledown-\ p' - a_\infty^2\rho'$; $-\blacksquare-$, $\rho u_i u_j$ spectrum. (*a*) $\theta = 30°$, (*b*) $\theta = 90°$.

For the Mach 2.0 cold jet in the 30° direction the cubic term is of the least importance at all frequencies. The linear term $L_2 = \rho'\overline{u}_i\overline{u}_j$ is of the most importance to the radiated far field sound for a 30° observer for $St \geqslant 0.5$, while L_1 dominates for $St < 0.5$. At 90° the linear term L_2 becomes of the least importance at all frequencies, while the two terms $L_1 = \overline{\rho}(\overline{u}_i u'_j + u'_i\overline{u}_j)$ and $Q_2 = \overline{\rho}u'_i u'_j$ contribute most to the overall spectrum, with the latter term dominating for $St < 0.5$. It is notable that the linear term L_2 swaps dominance completely with the pair (L_1, Q_2) when the observer angle is changed.

(We note that the ordering of the terms defined in (4.1) is made *in the acoustic far field* and may not apply to their distributions in the near field. This ordering will be dependent on observer location.)

For the Mach 1.0 heated jet (figure 6) at 30° we find the linear term L_2 dominates at all frequencies, with the quadratic term Q_2 being within 5 dB of L_2 over the available frequencies. The linear term L_1 is confined to $St \leqslant 0.1$, while the terms Q_1 and C are 8–10 dB and 10–15 dB, respectively, below the L_2 contribution. Above $St \approx 0.9$

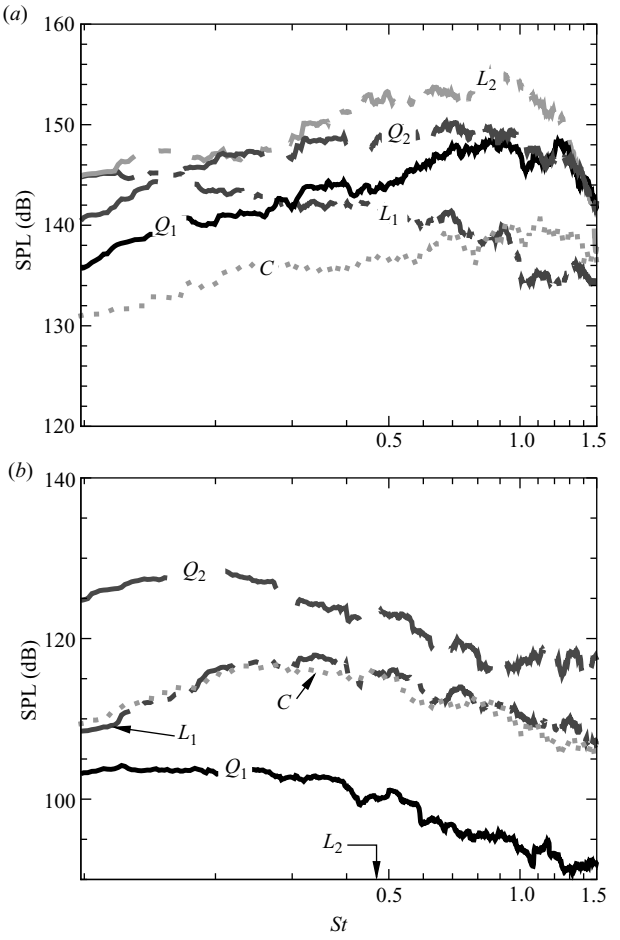

FIGURE 6. Component spectra contributing to the spectrum of $\rho u_i u_j$ for the jet M15TR230: $- \cdots - L_1$; $- \cdot - L_2$; —Q_1; $- - Q_2$; $\cdots C$; $-\blacktriangledown- \ p' - a_\infty^2 \rho'$; $-\blacksquare - \rho u_i u_j$ spectrum. Note the curve for L_2 in (*b*) lies below the figure scale. (*a*) $\theta = 30°$, (*b*) $\theta = 90°$.

we observe that $Q_1 \approx Q_2$. At 90° the linear term L_2 is far below the overall spectrum and does not appear on the scale of figure 6(*b*). For all frequencies the Q_1 quadratic term accounts for the majority of the overall $\rho u_i u_j$ spectrum, while the spectra of L_1 and C are similar but do not appear to contribute to the total.

The importance of the linear term L_2 at higher frequencies for the 30° observer deserves additional comment. Historically those terms proportional to $\overline{u}_i$, i.e. those that include the mean velocity, have been associated with the notion of 'shear noise' (Goldstein 1976) according to which the sound is generated by the interaction of fluctuations with the mean flow. Another association is that the linear terms are related to the normal mode instability waves found in axisymmetric jets (Michalke 1984). Based on linear stability theory it is expected that the Strouhal number of most amplified normal modes is approximately $St = 0.35$ for the Mach 2 cold jet and $St = 0.2$ for the Mach 1 heated jet. For both jets the estimated maximum unstable frequency is around $St = 0.55$. If we assume that L_2 is solely associated with these instability waves, then we would expect the L_2 spectrum to peak around $St = 0.35$;

ID	TID	U_j/a_∞	U_j/a_j	T_j/T_∞	M_c	Re^b	$N_r \times N_\theta \times N_x$
M09TR086	sp7[a]	0.83	0.90	0.86	0.43	88 000	$128 \times 32 \times 256$
M15TR230	sp39	1.47	0.97	2.30	0.58	84 000	$128 \times 32 \times 256$
M15TR056	sp62	1.47	1.95	0.56	0.83	336 000	$128 \times 32 \times 256$

[a]The conditions for run M09TR086 are approximately the same as those used by Tanna (1977).
[b]The Reynolds numbers are those used in the present LES and are not the same as in the experiments.

TABLE 2. Conditions of the simulations presented. All simulations are performed on a domain of size $(x, r) \in [0, 31]D \times [0, 12.5]D$. The nomenclature sp$N$, where N is an integer and listed in the 'TID' column, refers to conditions tabulated in Tanna (1977).

however, figures 5 and 6 do not exhibit this. There is a weak local maximum in the L_2 spectrum at $St = 0.3$ for the Mach 2 cold jet (figure 5*a*) and one at $St = 0.2$ for the heated jet (figure 6*a*).

Another possible cause of the dominance of L_2 is the presence of Mach waves. Although the jets are 'high-speed' in the sense that they have supersonic acoustic Mach number U_j/a_∞ they have purely subsonic convective Mach numbers, as noted in table 2 according to the definition $M_c = U_j/(a_j + a_\infty)$. A more precise measure of the the convection velocity of coherent structures in the jet is given by the two-point, two-time correlation $\langle uu \rangle$ shown in figure 7, where it is seen that the heated jet is purely subsonic. The unheated jet shows supersonic convection along the centreline but subsonic along the shear layer at $r = D/2$, thus opening the possibility of Mach waves. But, as for the instability waves, the spectral contact of the Mach waves would be expected to peak around $St = 0.3$. As discussed by Ffowcs Williams (1965) the Mach wave source for high-speed shear layers is the time derivative of $[\rho \partial \overline{u}_r/\partial y_r]$, where $\partial \overline{u}_r/\partial y_r$ is the projection of the mean velocity gradient tensor in the direction of the observer. As the velocity gradient is highest in the shear layer in which the density fluctuations have a spectral peak around $St = 0.3$ there is no mechanism to explain the observed higher peak frequency around $St = 1$. Further, note that Mohseni, Colonius & Freund (2002) observed a similar lack of Mach waves for their Mach 1.92 jet and low-speed jets appear to also have a strong linear component (Lew *et al.* 2007).

To explain the peak of L_2 at the higher frequency of $St \approx 1$ we must find a physical reason other than instability or Mach waves. The linearity of L_2 in the density fluctuations implies that the portion of the far field density spectrum due to L_2 will be proportional to $\omega^4 S_{\rho\rho}$ in the Fraunhaufer limit, ignoring any factors associated with the spatial integrals. Here $S_{\rho\rho}$ is the near field temporal spectrum of ρ':

$$S_{\rho\rho} = \int \langle \rho'(t)\rho'(t+\tau) \rangle \exp\{\mathrm{i}\omega\tau\} \, \mathrm{d}\tau.$$

For weakly compressible turbulence it is expected that $\rho'/\overline{\rho} \sim (u'/\overline{a})^2$ and, similarly, that $p'/\overline{p} \sim (u'/\overline{a})^2$. Thus $S_{\rho\rho} \sim \overline{\rho}^2 \overline{a}^{-4} S_{uu} S_{uu}$ functionally, so that the density and pressure fluctuation spectra are, to leading order in $u'/\overline{a}$, quadratic in the velocity spectra, a result consistent with that found for weakly compressible turbulence by Ristorcelli (1997). For the 30° observer, then, the term $\rho' \overline{u}_x \overline{u}_x$ dominates the six terms of L_2 and has a frequency dependence that is functionally similar to Q_2, the term quadratic in the velocity fluctuations. Such scaling may explain the trend observed in figures 5 and 6. Near field temporal spectra of ρ' and u'_x (not shown but available in Bodony 2004) further demonstrate this functional relation.

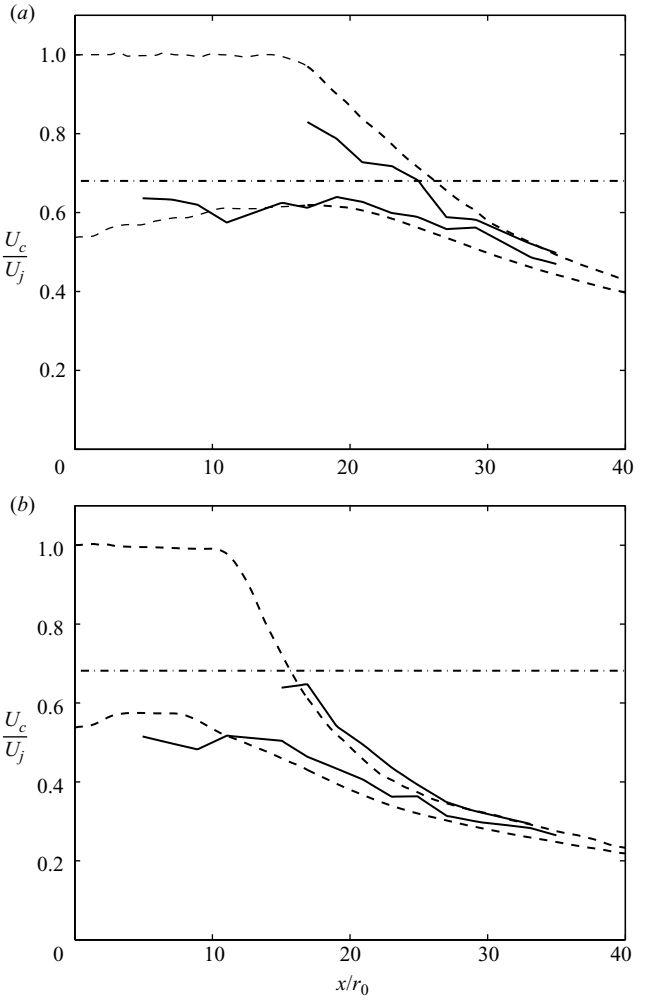

FIGURE 7. Convection velocities of $\langle u'u' \rangle$ for jets M15TR056 and M15TR230: ——, convection velocity U_c; — —, mean velocity $\langle u \rangle$. The two upper curves correspond to $r = 0$; the lower curves to $r = r_0$. The horizontal line is the ambient speed of sound a_∞ / U_j. (*a*) Jet M15TR056, (*b*) Jet M15TR230.

The dominance of the L_2 term for the 30° observer for the Mach 2.0 cold jet (for $St > 0.3$) and for the Mach 1.0 hot jet suggests an explanation for the strong correlation of $\rho u_i u_j$, via the x–x component, with $(p' - a_\infty^2 \rho')\delta_{ij}$. To see this, in the sound-generating region of the jet we observe that $\overline{u}_x \sim a_\infty$ (see figure 8 and the results in Bodony & Lele 2005). Likewise, from figures 5 and 6 and from the fact that $\overline{u}_x \gg \overline{u}_r$ we observe that $\rho u_i u_j$ is dominated by $\rho' \overline{u}_x \overline{u}_x$ for the 30° observer, which has strong cancellation with the term $p' - a_\infty^2 \rho'$. Figures 3 and 4 demonstrate this cancellation for $St \geqslant 0.4$, which is beyond the estimated frequency range of energetic linear instability modes.

We note that for the Mach 0.9 unheated jet the lower mean shear and consequently lower fluctuation root mean square values are not able to produce meaningful levels of ρ' (Bodony & Lele 2005) to be of consequence in the sound radiated to the far field, as inferred by Freund (2003).

At 90° the relevance of the L_2 is lowered, as the radial mean velocity component $\overline{u}_r$ is small relative to $\overline{u}_x$ and a_∞ in the radiating portion of the jet. The terms $L_1 \approx \overline{\rho}\,\overline{u}_x u_r'$, $Q_1 \approx \rho'\,\overline{u}_x u_r'$ and Q_2 thus remain possible contributors to the overall sound radiation. For the heated jet, with its low value of mean density in the sound-generating region, $L_{1,hot} < L_{1,cold}$, given since the velocity fluctuation levels are similar in magnitude between the cold and hot jets (Bodony & Lele 2005). For the cold jet at 90° we thus expect $L_1 > Q_1, Q_2$, which is observed for $St \geqslant 0.5$, while at lower frequencies $Q_2 > L_1$. For the heated jet at 90° the observation angle and low mean density imply that $Q_2 > Q_1, L_1$.

We note that the ordering arguments are made based on order-of-magnitude estimates in the acoustic far field and do not consider the frequency dependence of the fluctuations, other than the ω^2 contribution coming from the Green's function.

We also observe that in high-speed jets the modelling of the term $\rho u_i u_j$ with $\overline{\rho} u_i' u_j'$ is not justified. The fluctuations in density are important and must be accounted for in their contribution to T_{ij}.

4.2. *On Lilley's decomposition of T_{ij}*

From observations of the unheated jets at 90° it appears that both constituents of the $p' - a_\infty^2 \rho'$ term, namely term I and term II as defined in (3.1), are of approximately equal magnitude and combine to form the 'entropic' contribution to the SPL. For the heated jet, however, it is the enthalpy fluctuation term that takes precedence. This and the fact that, for the unheated jets at least, some cancellation occurs between the $\rho u_i u_j$ and $-[(\gamma-1)/2]\rho u_k u_k$ terms suggests that it is useful to prefer the decomposition due to Lilley (1974), which is the time-integrated form of his equation ((24) in his work)

$$T_{ij} = \underbrace{\rho u_i u_j - \frac{\gamma-1}{2}\rho u_k u_k \delta_{ij}}_{\text{momentum stress}} + \underbrace{a_\infty^2 \int \frac{\partial}{\partial x_k}\left[\rho u_k \left(\frac{h_\infty - h_s}{h_\infty}\right)\right]\delta_{ij}\,\mathrm{d}t}_{\text{enthalpy flux}} - \underbrace{\tau_{ij}}_{\text{viscous stress}}, \tag{4.2}$$

to better describe the roles of the various stresses to the sound spectra. The presence of the integral in time implies a non-local dependence of the sound field on the enthalpy fluxes. However, through the energy equation it is possible to write

$$\int \frac{\partial}{\partial x_k}\left[\rho u_k \left(\frac{h_\infty - h_s}{h_\infty}\right)\right]\mathrm{d}t$$

as $(\rho - \rho_\infty) - h_\infty^{-1}(\rho E - \rho_\infty E_\infty)$, where E is the total energy per unit mass, so that the appearance of the time integral is not unphysical. In using (4.2) the independence in modelling of the momentum and enthalpy fluctuations may be helpful. This conclusion is further borne out by the relative roles played by the momentum and 'entropy' terms for the hot Mach 1 jet.

At 30° the data suggest that Lilley's decomposition may also be beneficial. It was discussed previously that the leading terms of $\rho u_i u_j$ and $(p' - a_\infty^2 \rho')\delta_{ij}$ nearly completely cancel for the high-speed jets considered in this study. In Lilley's rearrangement of T_{ij} this cancellation occurs naturally within the momentum stress term, leaving the enthalpy flux contribution and the remaining momentum stress terms. As the arguments made for this cancellation are general, we would expect this conclusion to hold for other high-speed jets with $U_j \geqslant a_\infty$ up to those jets with $M_j > 2.5$, where Mach wave radiation becomes important.

4.3. *On the quieting of high-speed jets with heating*

For the two jets with the same exit velocity but different temperatures it is interesting to consider the reason, or reasons, why the heated jet is quieter. Although the heated jet has slightly increased fluctuation levels relative to the unheated jet the sound spectra are everywhere reduced. Microphone data has been used to observe a reduction in acoustic source volume (Morfey, Szewczyk & Tester 1978) in a heated jet, consistent with our previous data analysis (Bodony & Lele 2005).

The combination of the heated jet's lower mean density and the strong anti-correlation between the momentum and entropy terms are, from the Lighthill analogy perspective, the predominant reasons why high-speed heated jets are quieter compared to unheated jets at the same velocity. The impact of the lower mean density on the strength of the overall source has been well known for some time (Goldstein 1976; Morfey *et al.* 1978); the data presented herein supports this conclusion. Additionally, however, the correlation between the momentum and entropy terms causes additional cancellation in the far field.

It is interesting to hypothesize why, on the other hand, low-speed jets, with $U_j/a_\infty < 0.7$, become louder when heated. Based on the present results we would expect that, similar to the high-speed jets, the mean jet density and the convection velocity reduce when a low-speed jet is heated. Both of these effects appear to reduce the radiated noise. However, because the jet velocity is less than the ambient speed of sound, $\rho'\overline{u}_x^2 \sim \rho' a_\infty^2$ can never occur; so these two terms will not cancel. Instead, the increased levels of ρ' with heating suggest that the linear term $\rho'\overline{u}_i\overline{u}_j$ may become important and contribute to the increased radiated sound towards angles near the jet axis, along with the entropy term. The data of Lew *et al.* (2007) partially support this claim, but they did not explicitly measure the contribution of $\rho'\overline{u}_i\overline{u}_j$.

5. Conclusions

Based upon the investigation of the space–time databases provided by three LESs of high-speed turbulent jets, the Lighthill's acoustic analogy was examined. It was found that the Lighthill predictions agreed reasonably well with the directly computed radiated sound for jets of Mach numbers 0.9 (cold), 1.0 (hot) and 2.0 (cold). Investigation of the sound spectra showed that the momentum contribution due to $\rho u_i u_j$ was dominant at 90°, but its overall effect was dependent on cancellation with the entropy component $[p - p_\infty - a_\infty^2(\rho - \rho_\infty)]\delta_{ij}$ at 30°. In the cold Mach 0.9 jet the momentum stress was the determining factor for the sound spectra; at higher jet velocities this contribution was tempered by the $-[(\gamma - 1)/2]\rho u_k u_k \delta_{ij}$ portion of the entropy term for the cold jet and by the 'enthalpy flux' term for the heated jet. Modelling of the sound sources is made easier by considering the combined term $\rho u_i u_j - [(\gamma - 1)/2]\rho u_k u_k \delta_{ij}$ separate from the enthalpy flux, due to Lilley (1974), as the latter term is more important for heated jets. At 30° the original Lighthill (1952) momentum and entropic portions of T_{ij} are not independent, as the leading-order contributions from these two terms cancel. Moreover their spectra are not qualitatively similar to the far field pressure spectrum due to the importance of density fluctuations associated with the compressibility of the turbulence with the jet. That high-speed jets are quieter when heated (keeping the jet velocity constant) appears to be due to, in the Lighthill acoustic analogy context, a reduced sound-generating volume and increased cancellation between $\rho u_i u_j$ and the entropy term.

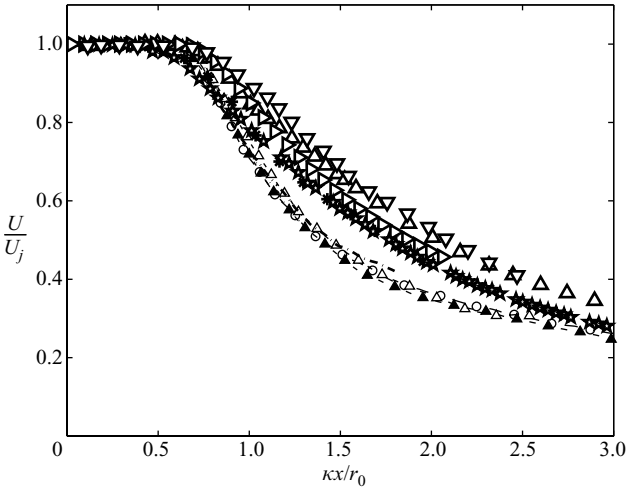

FIGURE 8. Centreline axial velocity in scaled and shifted Witze coordinates. Numerical data: $-\circ-$, M09TR086; $-\triangle-$, M15TR056; $-\blacktriangle-$, M15TR230; $-\cdot-$, Freund (2001); $--$, Bogey *et al.* (2003). Experimental data: $*$, Tanna (1977) (M09TR086); ∇, Arakeri *et al.* (2003); $\star$, Zaman (1986); $\triangleright$, Δ, Bridges & Wernet (2003);

This work is funded, in part, by the Aeroacoustics Research Consortium and the Center for Turbulence Research. Computer resources were provided by the U.S. Department of Defense through contract AFOSR F49620-01-1-0138. The authors thank Professor J. Freund, of the University of Illinois at Urbana-Champaign, for access to his data. An earlier, limited version of this article appeared as conference paper AIAA-2005-3041 and was presented at the AIAA/CEAS Aeroacoustics Conference and Exhibit in Monterey, CA, 22–25 May 2005.

Appendix. Validation of LES predictions and the Lightill-integrated far field spectrum

This paper is concerned with the data from those jets originally presented in Bodony & Lele (2005) having $M_j \geqslant 0.9$, which include two unheated jets and one heated jet. A brief summary of the simulations is given in this Appendix to establish the validity of the LES predictions.

A.1. *Summary of LES results*

For the jet conditions listed in table 1 LESs were carried out in cylindrical coordinates for the filtered, compressible equations of motion using Reynolds-averaged variables 31 diameters in the axial direction and 25 diameters in the radial direction. The dynamic Smagorinsky model (Germano *et al.* 1991) was used to close the subgrid scale stresses. Sixth-order optimized compact finite difference schemes were used in the radial and axial directions; Fourier spectral differencing was used in the azimuthal direction. Time integration used the low-dispersion, low-dissipation Runge–Kutta scheme of Stanescu & Habashi (1998). Forcing and absorbing sponges (Bodony 2006) provide boundary conditions on the computational boundaries. For all boundaries the sponges absorb, without reflection, the outgoing vortical, entropic and acoustic waves. At the inflow boundary the sponge also induces jet unsteadiness by forcing disturbances formed by a normal mode solution of the linearized stability equations for a spatially growing disturbance, on the inflow mean flow profile. Azimuthal

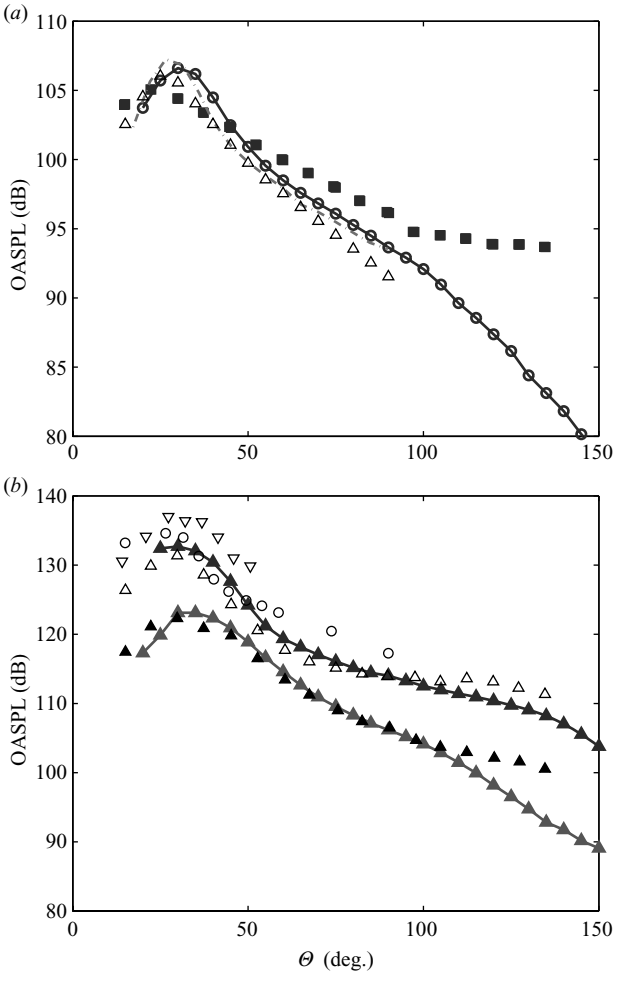

FIGURE 9. OASPL predictions at $100D_j$ for all three cases. Numerical data: — ○ — M09TR086; — △ — M15TR056; —▲— M15TR230; — · — Freund (2001). Experimental data: (*a*) Mach 0.9 cold jet (M09TR086): ■ Tanna (1977) (M09TR086); Δ Stromberg *et al.* (1980). (*b*) High-speed jets: ▲ Tanna (1977) (M15TR230); Δ Tanna (1977) (M15TR056); ○ Troutt & McLaughlin (1982) (cold, $M_j = 2.0$, $Re = 5.2 \times 10^6$); ∇ Troutt & McLaughlin (1982) (cold, $M_j = 2.1$, $Re = 7.0 \times 10^5$).

mode number combinations, including $n = \pm 1, \ldots, \pm 4$, are random walked in time to provide approximate broadband forcing without generating unphysical noise; the axisymmetric mode was not explicitly forced. The forcing amplitude, when summed over all modes, was $u_{r.m.s.}/U_j = 0.03$. Consequences of this type of inflow condition are discussed in Bodony & Lele (2008).

The initial mean flow profile, specified at $x/r_0 = 0$, was of the form

$$\frac{U}{U_j} = \frac{1}{2}\left(1 - \tanh\left[\frac{1}{4\theta_0}\left\{\frac{r}{r_0} - \frac{r_0}{r}\right\}\right]\right),$$

where θ_0, the initial momentum thickness, is a parameter. In all calculations $\theta_0/D_j = 0.045$. Assuming constant static pressure, fixed stagnation temperature and known jet centreline temperature the density was found from the equation of

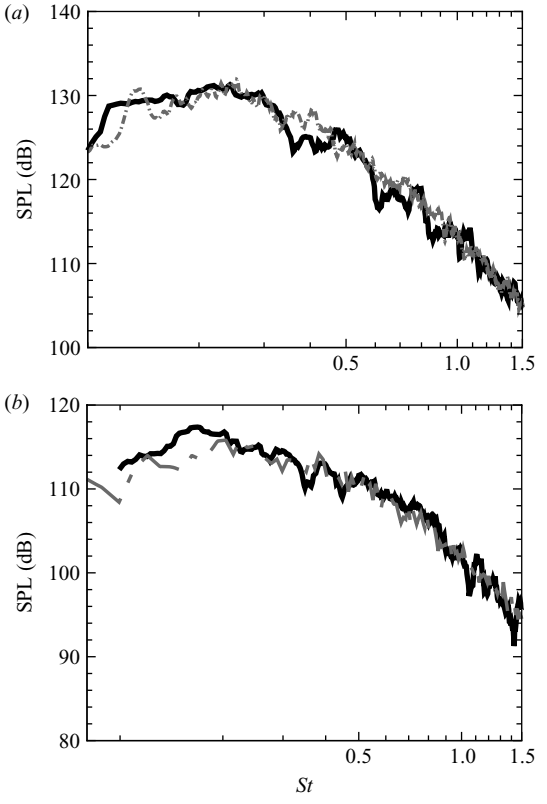

FIGURE 10. Narrowband spectra at $\mathscr{R} = 30D_j$ for the Mach 0.9 unheated jet M09TR086: — Lighthill (total); — · — Kirchhoff Surface. (*a*) $\theta = 30°$, (*b*) $\theta = 90°$.

state of an ideal gas. The reference solution used in the sponge zones was found from Reynolds-averaged Navier–Stokes solutions of the parabolized Navier–Stokes equations, using the v^2-f turbulence model (Choi & Lele 2001). A schematic of the computational domain, with sponge zones identified, is given in figure 1. Also shown in figure 1 are the binding cylindrical surfaces of the Kirchhoff surface used to extrapolate the sound to the far field, beyond the LES computational domain. Set at a distance of $R_s = 5D_j$ the Kirchhoff surface predictions are insensitive to the choice of R_s. The cylindrical surface is open with the upstream and downstream surfaces ignored. Although their absence may be accounted for, as in Freund, Lele & Moin (1996), the current results are instead restricted to polar angles in the range of $30° \leqslant \Theta \leqslant 150°$.

Figure 8 shows the centreline axial velocity U as a function of axial position, using the Witze (1974) scaling with $\kappa = 0.08(1 - 0.16M_j)(\rho_\infty/\rho_j)^{0.22}$ to remove the jets' axial elongation with increasing M_j. The jets have also been translated axially to have a common potential core length of $x_c/r_0 = 0.7[\kappa^2(\rho_\infty/\rho_j)]^{-1/2}$. In these coordinates the present calculations, along with those of Freund (2001) and of Bogey, Bailly & Juvé (2003) collapse onto a single curve which over-predicts the centreline velocity decay rate as measured by Tanna (1977) and others. The increased rate of change of U with x is believed to be caused by the relatively thick initial shear layers of the calculations compared with those found in experiment of $\theta_0 \sim 10^{-3}D_j$ (Viswanathan & Clark 2004). From the centreline axial velocity root mean square (not shown) it is found that

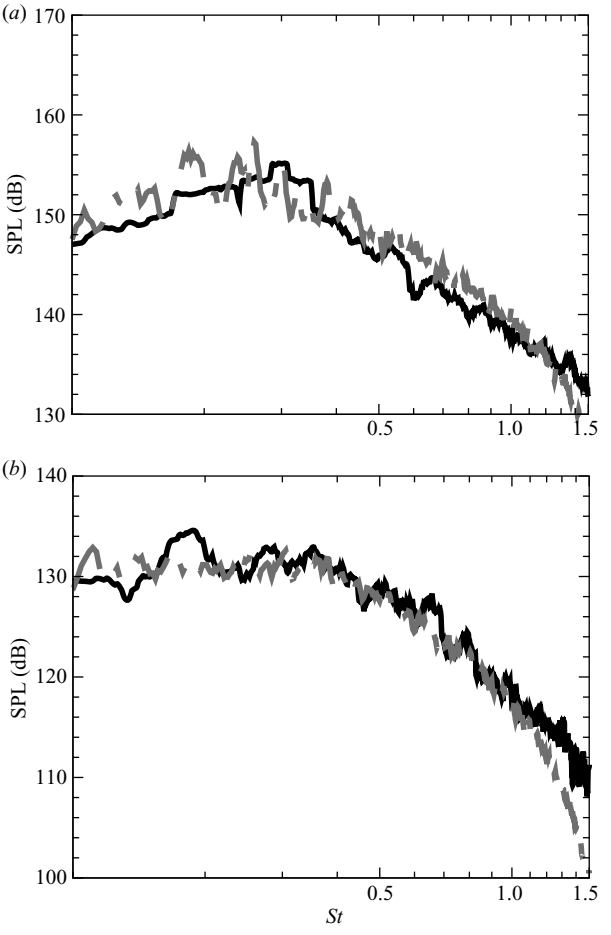

FIGURE 11. Narrowband spectra at $\mathscr{R} = 30D_j$ for the Mach 2.0 unheated jet M15TR056: — Lighthill (total); — · — Kirchhoff Surface. (*a*) $\theta = 30°$, (*b*) $\theta = 90°$.

the LES data over-predicts the experimental data by approximately $0.01U_j$ (3–4%). The discrepancy between the numerical and experimental data is believed to be related to the influence of the initially thick shear layers (Bodony & Lele 2008).

The OASPL predictions of the calculations are shown in figure 9(*a*) for the Mach 0.9 cold jet and in figure 9(*b*) for the $M_a \equiv U_j/a_\infty = 1.5$ heated and unheated jets. The numerical data is compared with the experimental data of Tanna (1977) and the published data of Freund (2001) along with the experimental data of others. In figure 9(*a*) the numerical predictions (LES and DNS) are 2–3 dB higher relative to Tanna's measurements but are consistent with the lower Reynolds number jet of Stromberg *et al.* (1980). There is general agreement with the peak OASPL value, its location in Θ and the roll-off away from the peak. Beyond $\Theta = 100°$ the LES calculations significantly under-predict the upstream-radiated sound. For the higher speed jets of figure 9(*b*) the OASPL predictions are within the scatter of the experimental data. When the jet is kept at constant velocity U_j and heated, the sound levels drop at all angles, and the peak radiation direction moves upstream. The cold high-speed jet is more directive than the heated jet with the same velocity as seen in

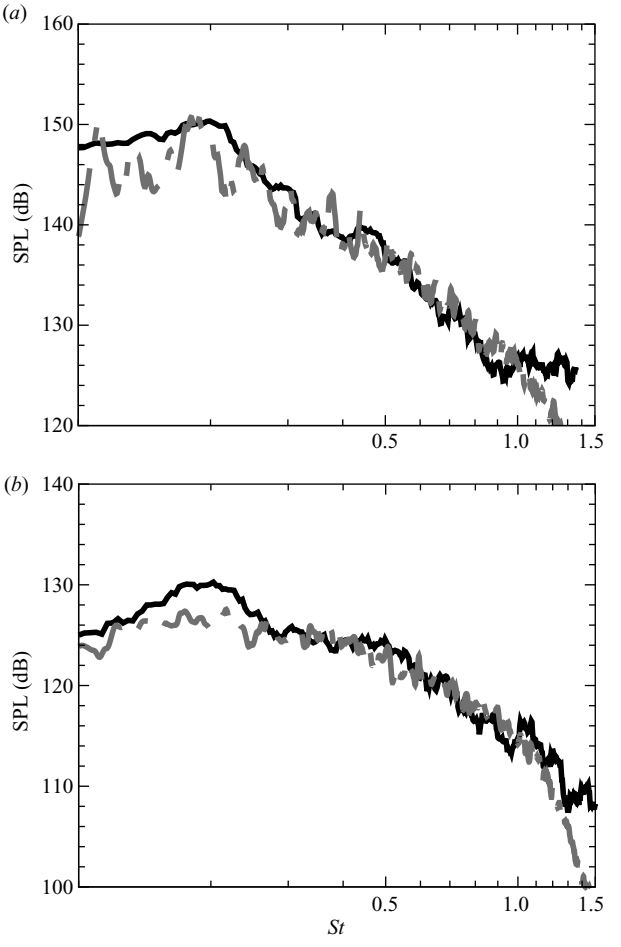

FIGURE 12. Narrowband spectra at $\mathscr{R} = 30D_j$ for the Mach 1.0 heated jet M15TR230: — Lighthill (total); — · — Kirchhoff Surface. (*a*) $\theta = 30°$, (*b*) $\theta = 90°$.

both the numerical and experimental data. The present LES predictions significantly under-predict the sound for $\Theta > 100°$. Acoustic spectral comparisons between the present LES and experimental jets are given in Bodony & Lele (2005).

Application of the integral form of Lighthill's analagy (2.4) for the Mach 0.9 unheated jet is shown for the two observer angles of 30° and 90° at a distance of $30D_j$ in figure 10. The Kirchhoff surface predictions for the same jet at the corresponding angles are also shown for comparison. There is reasonable agreement at both angles within the statistical uncertainty of the data. The peak SPL and the corresponding peak frequency are captured in the Lighthill integrations. (Freund 2003, for the 30° prediction, saw similar agreement with his DNS database.) Similar spectral shapes are seen in both prediction methods at each angle.

In figure 11 the Lighthill and Kirchhoff surface predictions are repeated for the Mach 2 unheated jet. As with the near-sonic cold jet the two sound predictions are similar for the range of Strouhal numbers available. The peak SPL and Strouhal number are captured as is the spectral shape for all frequencies. At 30° the Lighthill-predicted spectrum is 2 dB below the Kirchhoff spectrum for $0.4 \leqslant St \leqslant 1.0$. As

$St \rightarrow 1.5$ the predictions begin to differ due to grid resolution limitations with the Lighthill prediction being the higher. Our Kirchhoff surface data are not reliable beyond $St = 1.2$ for this jet.

The Mach 1 heated jet results are shown in figure 12 in which, again, the two methods yield similar predictions over a range of frequencies. For both angles the Lighthill prediction shows an over-prediction for $St < 0.2$, although the Kirchhoff surface data show increased oscillations in SPL at these frequencies, indicative of the limited statistical sample. The peak frequency appears to be closer to $St = 0.2$ at this operating condition for each angle.

REFERENCES

Andersson, N., Eriksson, L.-E. & Davidson, L. 2005*a* Effects of inflow conditions and subgrid model on LES for turbulent jets. AIAA Paper 2005-2925, presented at the 11th AIAA/CEAS Aeroacoustics Conference and Exhibit, 23–25 May, Monterey, CA, USA.

Andersson, N., Eriksson, L.-E. & Davidson, L. 2005*b* Large-eddy simulation of subsonic turbulent jets and their radiated sound. *AIAA J.* **43** (9), 1899–1912.

Arakeri, V. H., Krothapalli, A., Siddavaram, V., Alkislar, M. & Lourenco, L. 2003 On the use of microjets to suppress turbulence in a Mach 0.9 axisymmetric jet. *J. Fluid Mech.* **490**, 75–98.

Barré, S., Bogey, C. & Bailly, C. 2006 Computation of the noise radiated by jets with laminar/turbulent nozzle-exit conditions. AIAA Paper 2006-2443, presented at the 12th AIAA/CEAS Aeroacoustics Conference and Exhibit 8–10 May, 2006, Cambridge, MA, USA.

Bastin, F., Lafon, P. & Candel, S. 1997 Computation of jet mixing noise due to coherent structures: plane jet case. *J. Fluid Mech.* **335**, 261–304.

Bodony, D. J. 2004 Aeroacoustics of turbulent free shear flows. PhD thesis, Stanford University, Stanford, CA.

Bodony, D. J. 2006 Analysis of sponge zones for computational fluid mechanics. *J. Comp. Phys.* **212**, 681–702.

Bodony, D. J. & Lele, S. K. 2005 On using large-eddy simulation for the prediction of noise from cold and heated turbulent jets. *Phys. Fluids* **17**, 085103.

Bodony, D. J. & Lele, S. K. 2008 Current status of jet noise predictions using large-eddy simulation. *AIAA J.* **46** (2), 364–380.

Boersma, B. J. & Lele, S. K. 1999 Large eddy simulation of a Mach 0.9 turbulent jet. AIAA Paper 1999-1874, presented at the 5th AIAA/CEAS Aeroacoustics Conference, 10–12 May, Bellevue, WA, USA.

Bogey, C. & Bailly, C. 2003 LES of a high Reynolds, high subsonic jet: effects of the subgrid modellings on flow and noise. AIAA Paper 2003-3557, presented at the 16th AIAA Computational Fluid Dynamics Conference, June 23–26, Orlando, FL, USA.

Bogey, C. & Bailly, C. 2005 Effects of inflow conditions and forcing on subsonic jet flows and noise. *AIAA J.* **43** (5), 1000–1007.

Bogey, C. & Bailly, C. 2007 An analysis of the correlations between the turbulent flow and the sound pressure fields of subsonic jets. *J. Fluid Mech.* **583**, 71–97.

Bogey, C., Bailly, C. & Juvé, D. 2000 Computation of the sound radiated by a 3-D jet using large eddy simulation. AIAA Paper 2000-2009, presented at the 6th AIAA/CEAS Aeroacoustics Conference, Lahaina, HI, USA.

Bogey, C., Bailly, C. & Juvé, D. 2003 Noise investigation of a high subsonic, moderate Reynolds number jet using a compressible LES. *Theor. Comp. Fluid. Dyn.* **16**, 273–297.

Bridges, J. & Wernet, M. P. 2003 Measurements of the aeroacoustic sound source in hot jets. AIAA Paper 2003-3130, presented at the 9th AIAA/CEAS Aeroacoustics Conference and Exhibit, 12–14 May, Hilton Head Island, SC, USA.

Brusniak, L., Shur, M. L. & Spalart, P. R. 2006 Phased array imaging of jet noies sources in a large-eddy simulation. AIAA Paper 2006-2444, presented at the 12th AIAA/CEAS Aeroacoustics Conference, 08–10 May, Cambridge, MA, USA.

Choi, M.-R. & Lele, S. K. 2001 Prediction of shock-cell structure using parabolized stability equations. AIAA Paper 2001-0744, presented at the 39th Aerospace Sciences Meeting and Exhibit, 8–11 January, Reno, NV, USA.

Constantinescu, G. S. & Lele, S. K. 2001 Large eddy simulation of a nearly sonic turbulent jet and its radiated noise. AIAA Paper 2001-0376, presented at the 39th Aerospace Sciences Meeting and Exhibit 8–11 January 2001, Reno, NV.

Crighton, D. G. 1975 Basic principles of aerodynamic noise generation. *Prog. Aerospace Sci.* **16** (1), 31–96.

Ffowcs Williams, J. E. 1965 The mach wave field radiated by supersonic turbulent shear flows. *J. Fluid Mech.* **21** (4), 641–657.

Freund, J. B. 2001 Noise sources in a low-Reynolds-number turbulent jet at Mach 0.9. *J. Fluid Mech.* **438**, 277–305.

Freund, J. B. 2002 Turbulent jet noise: shear noise, self-noise, and entropic contributions. AIAA Paper 2002-2423, presented at the 8th AIAA/CEAS Aeroacoustics Conference & Exhibit, 17–19 June, Breckenridge, CO, USA.

Freund, J. B. 2003 Noise-source turbulence statistics and the noise from a Mach 0.9 jet. *Phys. Fluids* **15** (6), 1788–1799.

Freund, J. B., Lele, S. K. & Moin, P. 1996 Calculation of the radiated sound field using an open Kirchhoff surface. *AIAA J.* **34** (5), 909–916.

Gamet, L. & Estivalezes, J. L. 1998 Application of large-eddy simulations and Kirchhoff method to jet noise prediction. *AIAA J.* **36** (12), 2170–2178.

Germano, M., Piomelli, U., Moin, P. & Cabot, W. H. 1991 A dynamic subgrid-scale eddy viscosity model. *Phys. Fluids* A **3** (7), 1760–1765.

Goldstein, M. E. 1976 *Aeroacoustics*. McGraw-Hill.

Goldstein, M. E. 2003 A generalized acoustic analogy. *J. Fluid Mech.* **488**, 315–333.

Isaacson, E. & Keller, H. B. 1966 *Analysis of Numerical Methods*. Dover.

Khavaran, A., Bridges, J. & Freund, J. B. 2002 A parametric study of fine-scale turbulence mixing noise. AIAA Paper 2002-2419, presented at the 8th AIAA/CEAS Aeroacoustics Conference, June 17–19, Breckenridge, CO, USA.

Lew, P.-T., Blaisdell, G. A. & Lyrintzis, A. S. 2007 Investigation of noise sources in turbulent hot jets using large eddy simulation data. AIAA Paper 2007-0016, presented at the 45th Aerospace Sciences Meeting and Exhibit 8–11 January 2007, Reno, NV, USA.

Lighthill, M. J. 1952 On sound generated aerodynamically. Part I. General theory. *Proc. R. Soc. Lond.* A **211**, 564–587.

Lilley, G. M. 1974 On the noise from jets. *Tech. Rep.* AGARD CP-131. Advisory Group for Aerospace Research and Development.

Michalke, A. 1984 Survey on jet instability theory. *Prog. Aerospace Sci.* **21**, 159–199.

Mohseni, K., Colonius, T. & Freund, J. B. 2002 An evaluation of linear instability waves as sources of sound in a supersonic turbulent jet. *Phys. Fluids* **14**, 3593–3600.

Morfey, C. L., Szewczyk, V. M. & Tester, B. J. 1978 New scaling laws for hot and cold jet mixing noise based on a geometric acoustics model. *J. Sound Vib.* **61** (2), 255–292.

Panda, J. & Seasholtz, R. G. 2002 Experimental investigation of density fluctuations in high-speed jets and correlation with generated noise. *J. Fluid Mech.* **450**, 97–130.

Panda, J., Seasholtz, R. G., Elam, K. A., Mielke, A. F. & Eck, D. G. 2004 Effect of heating on turbulent density fluctuations and noise generation from high speed jets. AIAA Paper 2004-3016, presented at the 10th AIAA/CEAS Aeroacoustics Conference & Exhibit, 10–12 May, Manchester, UK.

Rembold, B. & Kleiser, L. 2004 Noise prediction of a rectangular jet using large-eddy simulation. *AIAA J.* **42** (9), 1823–1831.

Ristorcelli, J. R. 1997 A pseudo-sound constitutive relationship for the dilatational covariances in compressible turbulence. *J. Fluid Mech.* **347**, 37–70.

Saiyed, N. H., Mikkelsen, K. L. & Bridges, J. E. 2003 Acoustics and thrust of quiet separate-flow high-bypass-ratio nozzles. *AIAA J.* **41** (3), 372–378.

Samanta, A., Freund, J., Wei, M. & Lele, S. K. 2006 Robustness of acoustic analogies for predicting mixing layer noise. *AIAA J.* **44** (11), 2780–2786.

Shur, M., Spalart, P. R. & Strelets, M. K. 2005*a* Noise prediction for increasingly complex jets. Part I. Methods and tests. *Intl J. Aeroacous.* **4** (3–4), 213–246.

Shur, M., Spalart, P. R. & Strelets, M. K. 2005*b* Noise prediction for increasingly complex jets. Part II. Applications. *Intl J. Aeroacous.* **4** (3–4), 247–266.

Shur, M. L., Spalart, P. R., Strelets, M. K. & Garbaruk, A. V. 2006 Further steps in LES-based noise prediction for complex jets. AIAA Paper 2006-0485, presented at the 44th AIAA Aerospace Sciences Meeting and Exhibit, 9–12 January, Reno, NV, USA.

Stanescu, D. & Habashi, W. G. 1998 2*N*-Storage low dissipation and dispersion Runge–Kutta schemes for computational aeroacoustics. *J. Comp. Phys.* **143**, 674–681.

Stromberg, J. L., McLaughlin, D. K. & Troutt, T. R. 1980 Flow field and acoustic properties of a Mach number 0.9 jet at a low Reynolds number. *J. Sound Vib.* **72**, 159–176.

Tam, C. K. W. & Auriault, L. 1999 Jet mixing noise from fine-scale turbulence. *AIAA J.* **37** (2), 145–153.

Tanna, H. K. 1977 An experimental study of jet noise. Part I. Turbulent mixing noise. *J. Sound Vib.* **50** (3), 405–428.

Troutt, T. R. & McLaughlin, D. K. 1982 Experiments on the flow and acoustic properties of a moderate-Reynolds-number supersonic jet. *J. Fluid Mech.* **116**, 123–156.

Uzun, A. & Hussaini, M. Y. 2007 Investigation of high frequency noise generation in the near-nozzle region of a jet using large eddy simulation. *Theor. Comp. Fluid. Dyn.* **21**, 291–321.

Viswanathan, K. & Clark, L. T. 2004 Effect of nozzle internal contour on jet aeroacoustics. *Intl J. Aeroacous.* **3**, 103–135.

Viswanathan, K., Shur, M. L., Spalart, P. R. & Strelets, M. K. 2007 Comparisons between experiment and large-eddy simulation for jet noise. *AIAA J.* **45** (8), 1652–1966.

Viswanathan, K., Shur, M. L., Spalart, P. R. & Strelets, M. K. 2008 Flow and Noise Predictions for Single and Dual-Stream Beveled Nozzles. *AIAA J.* **46** (3), 601–626.

Witze, P. O. 1974 Centerline Velocity Decay of Compressible Free Jets. *AIAA J.* **12** (4), 417–418.

Zaman, K. B. M. Q. 1986 Flow field and near and far sound field of a subsonic jet. *J. Sound Vib.* **106** (1), 1–16.